Journal of Crystal Growth 318 (2011) 683–686

Contents lists available at ScienceDirect

Journal of Crystal Growth

journal homepage: www.elsevier.com/locate/jcrysgro

Synthesis, structural and vibrational properties of microcrystalline $RbNd(MoO_4)_2$

V.V. Atuchin [a,*], O.D. Chimitova [b], T.A. Gavrilova [c], M.S. Molokeev [d], Sung-Jin Kim [b], N.V. Surovtsev [e], B.G. Bazarov [f]

[a] Laboratory of Optical Materials and Structures, Institute of Semiconductor Physics, SB RAS, Novosibirsk 630090, Russia
[b] Division of Nano Sciences, Department of Chemistry, Ewha Womans University, Seoul 120-750, Republic of Korea
[c] Laboratory of Nanodiagnostics and Nanolithography, Institute of Semiconductor Physics, SB RAS, Novosibirsk 630090, Russia
[d] Laboratory of Crystal Physics, Institute of Physics, SB RAS, Krasnoyarsk 660036, Russia
[e] Laboratory of Condensed Matter Spectroscopy, Institute of Automation and Electrometry, SB RAS, Novosibirsk 630090, Russia
[f] Laboratory of Oxide Systems, Baikal Institute of Nature Management, SB RAS, Ulan-Ude 670047, Russia

ARTICLE INFO

Available online 20 October 2010

Keywords:
A1. Crystal structure
A2. Solid state synthesis
B1. Molybdate

ABSTRACT

Rubidium neodymium dimolybdate, $RbNd(MoO_4)_2$, microcrystals have been fabricated by solid state synthesis at $T=550$–$600^{\circ}C$ by $t=324$ ks. Crystal structure of $RbNd(MoO_4)_2$ has been refined by Rietveld method in space group Pbcn with cell parameters $a=5.1772(1)$ Å, $b=18.7293(4)$ Å, and $c=8.2774(1)$ Å ($R_B=5.05\%$). The crystal structure of $RbNd(MoO_4)_2$ consists of layers of MoO_4 tetrahedrons corner-sharing with NdO_8 square antiprisms. These layers are perpendicular to *b*-axis of the unit cell. About 20 narrow Raman lines have been observed in Raman spectrum recorded for $RbNd(MoO_4)_2$ powder sample.

1. Introduction

Complex molybdates display a variety of crystal structures and possess useful electro-physical, optical and catalytic properties [1–8]. Double molybdates containing alkali and trivalent metals are well known in literature and belong to the wide crystal family $MLn(MoO_4)_2$ (M—alkali metal and Ln—lanthanide) having important properties and applications. The molybdates $MLn(MoO_4)_2$ are excellent Ln-doped laser hosts [9]. Due to strong distortion of MoO_6 octahedrons many molybdates are characterized by noncentrosymmetric crystal structure [1,2,10–14]. Complex molybdates containing Ln^{3+} ions in low-symmetry positions are promising for the creation of new effective laser mediums [14–18]. This study aims to synthesize the $RbNd(MoO_4)_2$ microcrystals and evaluate the morphological, structural and vibrational properties of the compound. Formation of binary molybdate $RbNd(MoO_4)_2$ was previously found in quasi-binary system Rb_2MoO_4–$Nd_2(MoO_4)_3$ [19].

2. Experimental

Middle-temperature solid state synthesis was applied to create the $RbNd(MoO_4)_2$ crystals. MoO_3 (99.9%), Rb_2CO_3 (99.99%) and Nd_2O_3 (>99.9%) were used as starting materials. Initially rubidium molybdate and neodymium molybdate were prepared by solid state reactions [20]. To avoid a loss of molybdenum oxide due to its high volatility, heat treatment of stoichiometric mixtures was started at $T=450\ ^{\circ}C$ and followed by step-wise increase in temperature up to $T=600$ (Rb_2MoO_4) and $800\ ^{\circ}C$ ($Nd_2(MoO_4)_3$). These molybdates were mixed and annealed at $T=550$–$600\ ^{\circ}C$ by time $t=324$ ks to yield $RbNd(MoO_4)_2$. The temperature was increased gradually with the step of $50\ ^{\circ}C$ and the reaction mixtures were calcinated for 180–360 ks at each annealing stage with intermittent grindings in every 72 ks. As a result of synthesis a lilac powder is formed, whose color is typical for neodymium-bearing oxides. Phase compositions of the products were evaluated by X-ray powder diffraction analysis with Bruker D8 ADVANCE instrument. Micromorphology and chemical composition were observed by SEM and EPMA with LEO 1430 device.

The X-ray powder patterns for the Rietveld analysis were collected at room temperature ($T=24\ ^{\circ}C$) with a Bruker D8 ADVANCE powder diffractometer in the Bragg–Brentano geometry and a linear Vantec detector (CuK_{α} radiation, step size 0.016°, counting time 2 s per step). The data were collected over the angle range $2\theta=5$–100°. Peak positions were determined with the program EVA available in the PC software package DIFFRAC-PLUS supplied from Bruker. X-ray patterns of the title compound were indexed using the program McMaille [21]. Almost all reflections were indexed in orthorhombic space group Pbcn with cell

* Corresponding author. Tel.: +7 383 3308889; fax: +7 383 3332771.
E-mail address: atuchin@thermo.isp.nsc.ru (V.V. Atuchin).

0022-0248/$ - see front matter © 2010 Elsevier B.V. All rights reserved.
doi:10.1016/j.jcrysgro.2010.09.076

Table 1
Main parameters of processing and refinement.

Space group	Pbcn
a (Å)	5.1772(1)
b (Å)	18.7293(4)
c (Å)	8.2474(1)
V (Å^3)	799.76(3)
2θ-interval range (deg)	5–100
Number of reflexions	411
Number of refinement parameters	28
R_B	5.05%
R_{DDM}	11.91%

parameters a=5.18 Å, b=18.73 Å and c=8.25 Å except several minor intensity peaks that could not be assigned definitely. $RbNd(MoO_4)_2$ is supposed to be isostructural to $TlPr(MoO_4)_2$; hence we use atomic coordinates in $TlPr(MoO_4)_2$ to refine the structure of $RbNd(MoO_4)_2$ [22]. All refinements and data processing have been performed by DDM program [23]. The pseudo-Voigt function was used to model the peak profiles. The thermal parameters of all ions were refined isotropically and had reliable values. The refinement of structure was stable and led to minimal R-factors. The main parameters of processing and refinement are reported in Table 1.

Unpolarized Raman scattering spectra were recorded from powder sample using a triple grating spectrometer TriVista 777 and a line of 532 nm of solid state laser (200 mW) at room temperature. Spectral resolution was ~1 cm^{-1} (FWHM).

3. Results and discussion

In Fig. 1 the morphology of final product is shown. Microcrystals are formed by slightly agglomerated plate-like crystals with typical dimensions $12\times6\times1$ μm^3 and smoothed edges. Crystal habit appears to be governed by a layered structure typical for $MLn(MoO_4)_2$-type molybdates.

Experimental (dots) and theoretical (lines) X-ray diffraction curves obtained for $RbNd(MoO_4)_2$ are shown in Fig. 2. A good relation between experimental and theoretical curves is evident. The atomic coordinates, isotropic thermal parameters and occupations of atom positions revealed for $RbNd(MoO_4)_2$ are presented in Table 2. A set of main bond lengths is shown in Table 3. The crystal structure refined is shown in Fig. 3. The crystal structure of $RbNd(MoO_4)_2$ consists of layers of MoO_4 tetrahedrons corner-sharing with NdO_8 square antiprisms. These layers are perpendicular to b-axis of the unit cell. The NdO_8 square antiprism shares edge with another NdO_8 antiprism; hence all of them build a rod along c-axis. Rubidium atoms are located between MoO_4–NdO_8 layers and coordinated by six oxygen ions. Since Mo ion has four short Mo−O lengths d(Mo−O)=1.72–1.85 Å (Table 3) and two very long Mo−O lengths d(Mo−O)=2.77–2.79 Å, polyhedron MoO_n may be represented as highly distorted octahedron.

Raman spectrum of $RbNd(MoO_4)_2$ crystals is shown in Fig. 4. About 20 narrow Raman lines were observed in the experimental spectrum. In the range of stretched vibrations of MoO_n polyhedra (800–1000 cm^{-1}) five lines were observed and this range is shown in detail in Fig. 5. The narrowest (FWHM is 6.4 cm^{-1}) and intensive line is detected at 936 cm^{-1}. This line can be considered as an analog of Mo=O stretch line of α-MoO_3 crystals (995 cm^{-1}) [24–26]. Two lines at 802 and 864 cm^{-1} with FWHM of 17 and 20 cm^{-1}, respectively, are evidently wider. The line of 819 cm^{-1} in Raman spectrum of α-MoO_3 crystal with width triple as large as that of 995 cm^{-1} line can be considered as a fingerprint for 802 and 864 cm^{-1} lines of $RbNd(MoO_4)_2$ crystal. We guess that the difference in the linewidths of 936 and 864 cm^{-1} lines relates to different contributions of Mo atoms. The distribution of Mo isotopes in natural abundance causes the distribution of vibrational frequencies if Mo atoms are involved in the vibration. Another interesting feature of Raman spectrum of $RbNd(MoO_4)_2$ crystal is the intense low-frequency mode at 50 cm^{-1} shown in Fig. 6. The low-frequency mode in the range 30–60 cm^{-1} is often found for crystals with layering structure (e.g. chalcogenides). This mode could correspond to elastic-like vibrations of the layer.

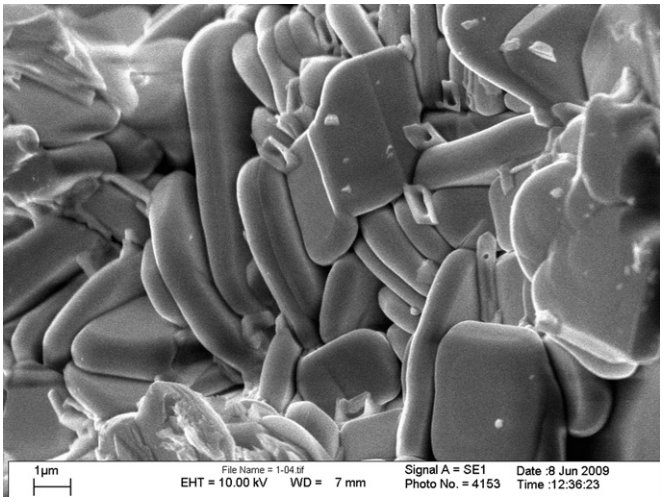

Fig. 1. SEM image of $RbNd(MoO_4)_2$ microcrystals.

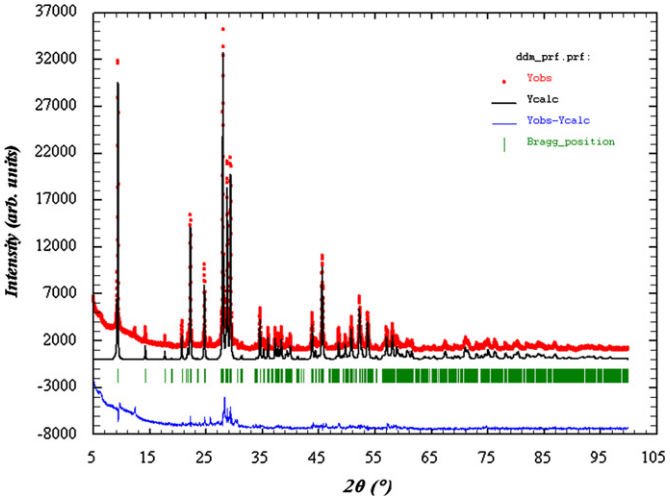

Fig. 2. X-ray diffraction pattern of $RbNd(MoO_4)_2$ at room temperature.

Table 2
Coordinates of atoms, isotropic thermal parameters (B_{iso}) and occupation of atom positions (p) of $RbNd(MoO_4)_2$ structure at T=24 °C.

Atom	p	X	Y	Z	B_{iso} (Å^2)
Rb	1.0	1/2	0.2675(2)	1/4	2.7(1)
Nd	1.0	0	0.0086(1)	1/4	2.0(1)
Mo	1.0	0.5214(8)	0.1014(1)	0.9791(3)	1.7(1)
O1	1.0	0.733(3)	0.103(1)	0.142(3)	1.3(6)
O2	1.0	0.731(3)	0.097(1)	0.817(2)	1.0(6)
O3	1.0	0.261(4)	0.035(1)	0.011(5)	3.5(8)
O4	1.0	0.411(4)	0.189(1)	0.979(2)	3.4(6)

Table 3
Main interatomic distances in structure of $RbNd(MoO_4)_2$ at $T=24$ °C.

Bond	Length (Å)
Rb – O4[a]	2.71(2)
Rb – O4	2.96(2)
Rb – O2	2.95(2)
Nd – O3	2.44(4)
Nd – O1	2.42(2)
Nd – O2	2.48(2)
Nd – O3[a]	2.74(4)
Mo – O2	1.72(2)
Mo – O4	1.74(2)
Mo – O1	1.74(2)
Mo – O3	1.85(2)

[a] $-x, y, 0.5-z$.

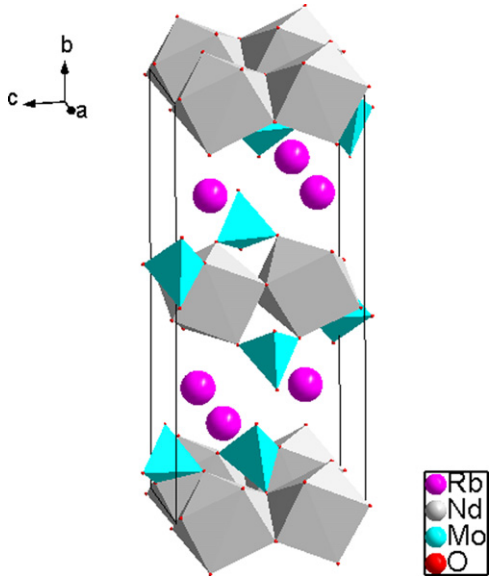

Fig. 3. Crystal structure of $RbNd(MoO_4)_2$ at room temperature.

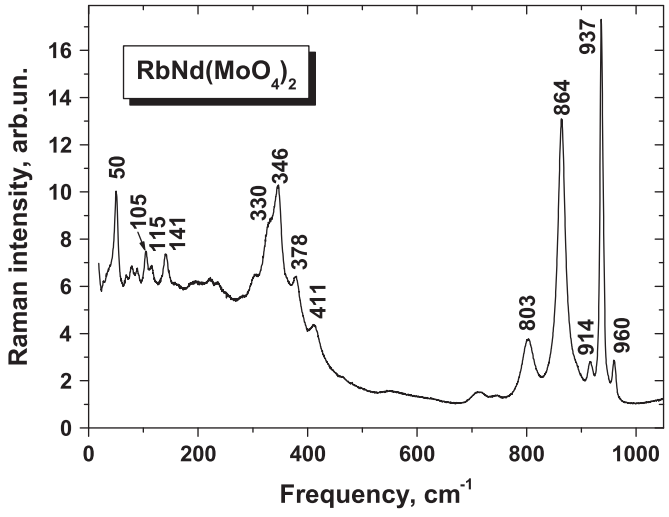

Fig. 4. Raman spectrum of $RbNd(MoO_4)_2$.

4. Conclusions

Binary molybdate $RbNd(MoO_4)_2$ is formed by solid state synthesis and crystal structure is refined by Rietveld method. The plate-like shape of $RbNd(MoO_4)_2$ microcrystals appeared to be governed by layered crystal structure, resulting in anisotropic microcrystal growth. Low-symmetry positions are found for Nd^{3+} ions. Spectroscopic parameters confirm layered character of the crystal lattice.

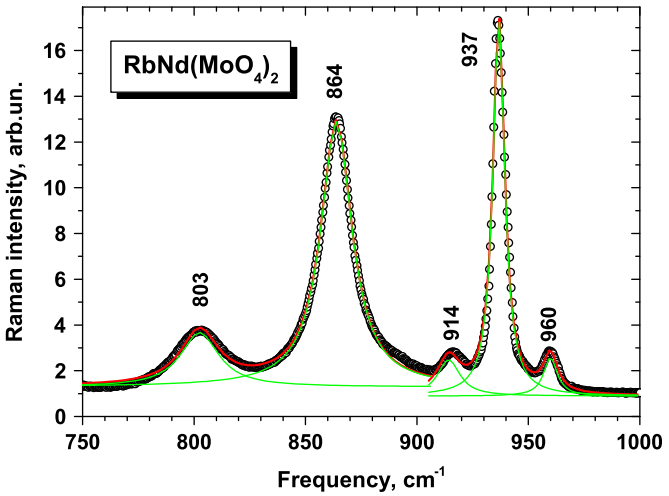

Fig. 5. Raman spectrum of $RbNd(MoO_4)_2$ in the range of Mo – O stretch vibrations with the fit by Lorentz functions.

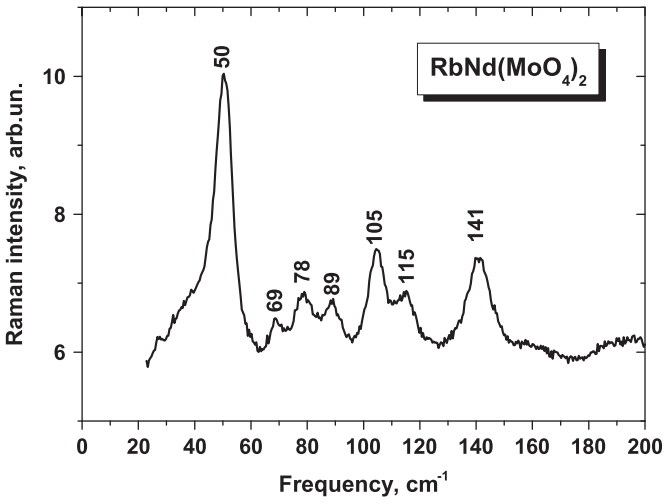

Fig. 6. Low-frequency part of Raman spectrum of $RbNd(MoO_4)_2$.

Acknowledgment

This study was partly supported by SB RAS (Grant 34).

References

[1] F.A. Schröder, Contributions to the chemistry of Mo and W: XIV. The Mo – O bond length/bond order relationship: a systematic treatment, Acta Crystallogr. B 31 (1975) 2294–2309.
[2] Kang Min Ok, P. Shiv Halasyamani, Distortions in octahedrally coordinated d^0 transition metal oxides: a continuous symmetry measures approach, Chem. Mater 18 (2006) 3176–3183.
[3] I.B. Troitskaia, T.A. Gavrilova, S.A. Gromilov, D.V. Sheglov, V.V. Atuchin, R.S. Vemuri, C.V. Ramana, Growth and structural properties of α-MoO_3 (010) microplates with atomically-flat surface, J. Mater. Sci. Eng. B 174 (1–3) (2010) 159–163.
[4] C.V. Ramana, I.B. Troitskaia, V.V. Atuchin, M. Ramos, D. Ferrer, Electron microscopy characterization of hexagonal molybdenum trioxide (MoO_3) nanorods, J. Vac. Sci. Technol. A 28 (4) (2010) 726–729.

[5] V.I. Voronkova, V.K. Yanovskii, E.P. Kharitonova, Oxygen-conducting crystals of $La_2Mo_2O_9$: growth and main properties, Crystallogr, Rep. 50 (5) (2005) 874–876.
[6] Lin Ma, Yuzeng Sun, Peng Gao, Yongkui Yin, Zengming Qin, Baibin Zhou, Controlled synthesis and photoluminescence properties of hierarchical $BaXO_4$ (X=Mo, W) nanostructures at room temperature, Mater, Lett 64 (10) (2010) 1235–1237.
[7] B.G. Bazarov, R.F. Klevtsova, O.D. Chimitova, L.A. Glinskaya, K.N. Fedorov, Yu.L. Tushinova, Zh.G. Bazarova, Phase formation in the Rb_2MoO_4–$Er_2(MoO_4)_3$–$Hf(MoO_4)_2$ system and the crystal structure of new triple molybdate $Rb_5ErHf(MoO_4)_6$, Russ. J. Inorg. Chem. 51 (5) (2006) 800–804.
[8] B.G. Bazarov, R.F. Klevtsova, Ts.T. Bazarova, L.A. Glinskaya, K.N. Fedorov, A.D. Tsyrendorhieva, O.D. Chimitova, Zh.G. Bazarova, Phase equilibria in the system Rb_2MoO_4–$R_2(MoO_4)_3$–$Hf(MoO_4)_2$ (R=Al, In, Sc, Fe(III)) and the crystal structure of double molybdate $RbFe(MoO_4)_2$, Russ. J. Inorg. Chem. 51 (7) (2006) 1111–1115.
[9] A.A. Kaminskii, Laser Crystals: Their Physics and Properties, Springer-Verlag, Berlin, 1981 456 pp. CAN 94:148230 AN 1981:148230 CAPLUS.
[10] Hyun-Seup Ra, Kang Min Ok, P. Shiv Halasyamani, Combining second-order Jahn–Teller distorted cations to create highly efficient SHG materials: synthesis, characterization, and NLO properties of $BaTeM_2O_9$ ($M=Mo^{6+}$ or W^{6+}), J. Am. Chem. Soc 125 (2003) 7764–7765.
[11] Weiguo Zhang, Xutang Tao, Chengqian Zhang, Zeliang Gao, Yongzhuan Zhang, Wentao Yu, Xiufeng Cheng, Xuesong Liu, Minhua Jiang, Bulk growth and characterization of a novel nonlinear optical crystal $BaTeMo_2O_9$, Cryst. Growth Design 8 (1) (2008) 304–307.
[12] V.V. Atuchin, B.I. Kidyarov, Classification and search for novel binary acentric molybdate and wolframate crystals, J. Korean Cryst. Growth Cryst. Technol. 12 (6) (2002) 323–328.
[13] V.V. Atuchin, B.I. Kidyarov, N.V. Pervukhina, Phenomenological modeling and design of new acentric crystals for optoelectronics, Comput. Mater. Sci. 30 (3-4) (2004) 411–418.
[14] E.V. Zharikov, C. Zaldo, F. Díaz, Double tungstate and molybdate crystals for laser and nonlinear optical applications, MRS Bull 34 (2009) 271–276.
[15] Alexander A. Kaminskii, Laser crystals and ceramics: recent advances, Laser Photon. Rev. 1 (2) (2007) 93–177.
[16] Yu-Qi Zou, Xue-Yuan Chen, Ding-Yuan Tang, Zun-Du Luo, Wen-Qin Yang, Investigation of the spectroscopic properties of acentric orthorhombic Nd^{3+}:$Gd_2(MoO_4)_3$ crystals, Opt. Commun. 167 (1999) 99–104.
[17] A. Méndez-Blas, M. Rico, V. Volkov, C. Zaldo, C. Cascales, Crystal field analysis and emission cross sections of Ho^{3+} in the locally disordered single-crystal laser hosts $M^+Bi(XO_4)_2$ (M^+=Li, Na; X=W, Mo), Phys. Rev. B 75 (2007) 174208.
[18] Weijie Guo, Yujin Chen, Yanfu Lin, Xinghong Gong, Zundu Luo, Yidong Huang, Spectroscopic analysis and laser performance of Tm^{3+}:$NaGd(MoO_4)_2$ crystal, J. Phys. D: Appl. Phys 41 (2008) 115409.
[19] M.V. Mokhosoev, E.I. Get'man, F.P. Alexeev, Binary molybdates of alkali and rare earth elements with $MeLn(MoO_4)_2$ composition, Dokl. Akad. Nauk SSSR 185 (2) (1969) 361–362.
[20] O.D. Chimitova, B.G. Bazarov, K.N. Fedorov, Zh.G. Bazarova, Phase relationships in the triple salt systems Rb_2MoO_4–$Ln_2(MoO_4)_3$ – $Hf(MoO_4)_2$, where Ln=La – Lu and new family of triple molybdates $Rb_5LnHf(MoO_4)_6$, Buryat State Univ. Bull. Ser. 1: Chem. 2 (2005) 37–40.
[21] A. Le Bail, Monte Carlo indexing with McMaille, Powder Diffr. 19 (3) (2004) 249–254.
[22] E.T. Khobrakova, V.A. Morozov, A.A. Belik, B.I. Lazoryak, E.G. Khaikina, O.M. Basovich, Structure of some thallium lanthanide double molybdates of composition $TlLn(MoO_4)_2$, Russ. J. Inorg. Chem. 49 (3) (2004) 444–450.
[23] L.A. Solovyov, Full-profile refienement by derivative difference minimization, J. Appl. Crystallogr. 37 (2004) 743–749.
[24] M.A. Py, K. Maschke, Intra- and interlayer contributions to the lattice vibrations in MoO_3, Physica B 105 (1981) 370–374.
[25] W.G. Chu, L.N. Zhang, H.F. Wang, Z.H. Han, D. Han, Q.Q. Li, S.S. Fan, Direct thermal oxidization evaporation growth, structure, and optical properties of single-crystalline nanobelts of molybdenum trioxide, J. Mater. Res. 22 (6) (2007) 1609–1617.
[26] Bin Yan, Zhe Zheng, Jixuan Zhang, Hao Gong, Zexiang Shen, Wei Huang, Ting Yu, Orientation controllable growth of MoO_3 nanoflakes: micro-Raman, field emission, and birefringence properties, J. Phys. Chem. C 113 (2009) 20259–20263.